

New analytical model of rotating black hole with dark matter halo: constraints from EHT observations and accretion disk

Uktamjon Uktamov^{a,f,d,*}, Sanjar Shaymatov^{b,c,g}, Bobomurat Ahmedov^{a,d,e,1}, Chengxun Yuan^a

^a*School of Physics, Harbin Institute of Technology, Harbin 150001, People's Republic of China*

^b*Institute of Fundamental and Applied Research, National Research University TIAME, Kori Niyoziy 39, Tashkent 100000, Uzbekistan*

^c*Institute for Theoretical Physics and Cosmology, Zhejiang University of Technology, Hangzhou 310023, China*

^d*Institute for Advanced Studies, New Uzbekistan University, Movarounnahr str. 1, Tashkent 100000, Uzbekistan*

^e*Institute of Theoretical Physics, National University of Uzbekistan, Tashkent 100174, Uzbekistan*

^f*Tashkent University of Applied Sciences, Gavhar Str. 1, Tashkent 100149, Uzbekistan*

^g*Tashkent State Technical University, Tashkent 100095, Uzbekistan*

Abstract

In this paper, we start from a static black hole (BH) immersed in a Dehnen-type dark matter (DM) halo and employ the Newman-Janis algorithm (NJA) to generate the rotating black hole solution with a dark matter halo. Also, we have checked the validity of the obtained space-time. Then we study optical properties of newly obtained rotating BH in DM halo, including the shadow's geometrical shape, deflection angle of light based Ono, Ishihara and Asada (OID) method, photon sphere and the dependence of the shadow radius on DM parameters. Additionally, assuming that spacetime of a supermassive black hole (SMBH) is described by the newly obtained rotating BH solution, we analyze the parameters of the model with shadow size estimates based on the Event Horizon Telescope (EHT) and Gravity collaboration observations of M87* and Sgr A* SMBHs. Then we have used Markov Chain Monte Carlo (MCMC) analysis to constrain DM parameters ρ_s , r_s and BH mass M , BH spin a , also we show that best-fit values for the parameters ρ_s , r_s are well agreement with previous results which indicate physical reasonability of the our model. Finally, we have analyzed the electromagnetic radiation flux of the rotating BH in the DM halo employing a ray tracing code.

Keywords: Dehnen-type dark matter halo, Newman-Janis algorithm, shadow, thin accretion disk

1. Introduction

One of the most fascinating predictions of General Relativity (GR) was the formation of black holes (BH) at the end state of evolution of massive stars and the assumption of existence of black holes in the center of galaxies [1, 2] which are responsible for high energetics of active galactic nuclei (AGN). The last decade was related to the triumphal revolutionary discoveries in relativistic astrophysics. However, these essential observations were not enough to explain the nature of the interaction between black holes and their surroundings. Therefore, understanding a behavior of the dark matter (DM) is crucial task in GR as there are enough evidence that BHs are surrounded by DM halo [3, 4]. Although, numerous efforts have been done to understand the nature of the DM halo, there is still only one way, gravitational interactions, to understand DM. Thus, finding exact analytical model for DM halo is utmost problem in GR. There are several analytical models, Einasto [5], Navarro-Frenk-White [6], Burkert [7] and the Dehnen model [8–13] to describe the interaction between BH and DM. In this work, we have chosen core model of the Dehnen-type dark matter halo

with the known exact analytical solution for static BH in DM halo and then using Newman-Janis algorithm we generated the novel rotating black hole solution with a dark matter halo.

Recent studies within the Dehnen-type DM halo framework have also examined interactions between DM and BHs from various viewpoints. In particular, these studies thoroughly examine black holes embedded within Dehnen-type dark matter halos exploring the influence of the DM halo on quasinormal modes, the BH shadow, and the photon sphere radius [14], alongside analyzing gravitational waveforms generated by periodic orbits [15] for the BH-Dehnen-type DM halo solution. Furthermore, the null geodesics and the thermodynamics of the effective BH-DM halo system were studied in [16], which is followed by an analysis that constrains the parameters of the DM halo [17].

Observations from the EHT, specifically images of supermassive black holes (SMBHs) Sgr A* and M87*, give opportunities to compare our theoretical findings with the real observational data [18–20]. In 2019, the EHT collaboration made a groundbreaking announcement by providing the first image of a black hole, a shadow-like representation of the supermassive black hole located in the center of the M87 galaxy [21]. Following, researchers from the EHT project unveiled an image of the black hole at the center of the Milky Way galaxy, known as Sgr A*, in 2022. In accordance with GR, the observed images of the two black holes, M87* and Sgr A*, are

*Corresponding author

Email addresses: uktam.uktamov11@gmail.com (Uktamjon Uktamov), sanjar@astrin.uz (Sanjar Shaymatov), ahmedov@astrin.uz (Bobomurat Ahmedov), yuancx@hit.edu.cn (Chengxun Yuan)

consistent with the properties predicted for a Kerr black hole. This agreement indicates that these black holes are effectively characterized by the Kerr metric, which serves as the solution to the Einstein field equations for a rotating black hole [22]. Although Kerr-like black holes emerging from modified gravity theories or including a DM halo are not fully validated due to the relative deviation in quadrupole moments and the current measurement uncertainties in spin or angular momentum, they cannot be completely excluded [23]. In recent years, the study of black hole shadows has attracted significant attention, particularly in the context of modified gravity theories [24]. Additionally, the exploration of spinning black holes has offered new insights into the optical properties and shadow features of these celestial objects [25]. Moreover, observational data, including those gathered by the EHT, have been crucial in constraining the range of theoretical parameters [26]. Consequently, one of the key challenges in modern astrophysics is evaluating the nature and existence of dark matter models using the data supplied by the EHT Collaboration. In this paper, we obtain constraints for the characteristic density ρ_s and the characteristic scale factor r_s of the DM halo using the observed data mentioned above.

The paper organized as follows: in Sec. 2, we generate a solution for a rotating BH surrounded by a Dehnen-type dark matter halo using Newman-Janis algorithm. In addition, event horizon of the rotating BH with a dark matter halo is analyzed in this section. The following null geodesics equations are derived using the Hamilton-Jacobi equation, the photon sphere around a rotating BH in a dark matter halo is analyzed, and finally, the shadow of the rotating BH in dark matter halo is investigated in Sec. 3. Subsequently, deflection angle of light by a rotating BH in DM halo and effect of the DM halo on deflection angle $\hat{\alpha}$ is investigated in Sec. 4. Then we obtain constraints for the BH parameters r_s and ρ_s applying the EHT and Gravity collaboration observation data to the obtained theoretical results in Sec. 5 and then we employed MCMC analysis to find best-fit values of the DM parameters ρ_s , r_s . Also we obtain image of the thin accretion in rotating BH surrounded by Dehnen-type DM halo in Sec. 6. Finally, we give our main conclusions in Sec. 7.

2. Spacetime of rotating black hole with the dark matter halo

The authors in [27] have found a novel static black hole solution surrounded by Dehnen-type dark matter halo in the form:

$$ds^2 = -f(r)dt^2 + \frac{1}{f(r)}dr^2 + r^2(d\theta^2 + \sin^2\theta d\phi^2), \quad (1)$$

where

$$f(r) = 1 - \frac{2M}{r} - 8\pi\rho_s r_s^2 \log\left(1 + \frac{r_s}{r}\right), \quad (2)$$

and ρ_s and r_s are the characteristic density and characteristic scale factor of the DM halo.

Now using Newman and Janis method (NJA) [28–32] we will generate rotating BH space-time in dark matter halo. To do it, we start with coordinate transformation from the Boyer-Lindquist (BL) coordinates (t, r, θ, ϕ) to the Eddington-Finkelstein

(EF) coordinates (u, r, θ, ϕ) :

$$du = dt - \frac{dr}{f(r)}, \quad (3)$$

which gives us:

$$ds^2 = -f(r)du^2 - 2dudr + r^2d\Omega^2, \quad (4)$$

with $d\Omega = d\theta^2 + \sin^2\theta d\phi^2$.

The contravariant components of the metric tensor in null EF coordinates can be written as:

$$g^{\mu\nu} = -l^\mu n^\nu - l^\nu n^\mu + m^\mu \bar{m}^\nu + m^\nu \bar{m}^\mu, \quad (5)$$

where null tetrads can be expressed after performing complex coordinate transformations $u \rightarrow u - ia \cos\theta$, $r \rightarrow r - ia \cos\theta$, and resulting $f(r) \rightarrow F(r, a, \theta)$, $r^2 \rightarrow \Sigma(r, a, \theta)$:

$$l^\mu = \delta_r^\mu \quad (6a)$$

$$n^\mu = \frac{1}{\sqrt{2\Sigma}} \left(\delta_\theta^\mu + ia \sin\theta (\delta_u^\mu - \delta_r^\mu) + \frac{i}{\sin\theta} \delta_\phi^\mu \right), \quad (6b)$$

$$\bar{m}^\mu = \delta_u^\mu - \frac{1}{2} F \delta_r^\mu, \quad (6c)$$

$$\bar{m}^\mu = \frac{1}{\sqrt{2\Sigma}} \left(\delta_\theta^\mu - ia \sin\theta (\delta_u^\mu - \delta_r^\mu) - \frac{i}{\sin\theta} \right). \quad (6d)$$

Finally, we can express a rotating black hole spacetime surrounded by Dehnen-type dark matter halo:

$$ds^2 = g_{tt}dt^2 + 2g_{t\phi}dtd\phi + g_{\phi\phi}d\phi^2 + g_{rr}dr^2 + g_{\theta\theta}d\theta^2, \quad (7)$$

with metric components:

$$g_{tt} = - \left[1 - \frac{2Mr + 2M_D r \log\left(1 + \frac{r_s}{r}\right)^{\left(1 + \frac{r_s}{r}\right)}}{\Sigma} \right], \quad (8a)$$

$$g_{rr} = \frac{\Sigma}{\Delta}, \quad (8b)$$

$$g_{t\phi} = -a \sin^2\theta \left[\frac{2Mr + 2M_D r \log\left(1 + \frac{r_s}{r}\right)^{\left(1 + \frac{r_s}{r}\right)}}{\Sigma} \right], \quad (8c)$$

$$g_{\phi\phi} = \sin^4\theta \left[\frac{r^2 + a^2}{\sin^2\theta} + \frac{a^2 \left(2Mr + 2M_D r \log\left(1 + \frac{r_s}{r}\right)^{\left(1 + \frac{r_s}{r}\right)} \right)}{\Sigma} \right], \quad (8d)$$

$$g_{\theta\theta} = \Sigma, \quad (8e)$$

where $M_D = \frac{4\pi\rho_s r_s^3}{1 + \frac{r_s}{r}}$ is the mass profile of the DM halo and:

$$\Sigma = r^2 + a^2 \cos^2\theta, \quad (9a)$$

$$\Delta = r^2 - 2Mr + a^2 - 2M_D r \log\left(1 + \frac{r_s}{r}\right)^{\left(1 + \frac{r_s}{r}\right)}. \quad (9b)$$

In Fig. 1, we have plotted the radial dependence of the Δ function. From these graphics plotted in Fig. 1, one can easily conclude, that there are two horizons for larger values of the BH parameters r_s and ρ_s from the top panels of Fig. 1, but enlarging spin a of the BH causes the disappearance of the event horizon

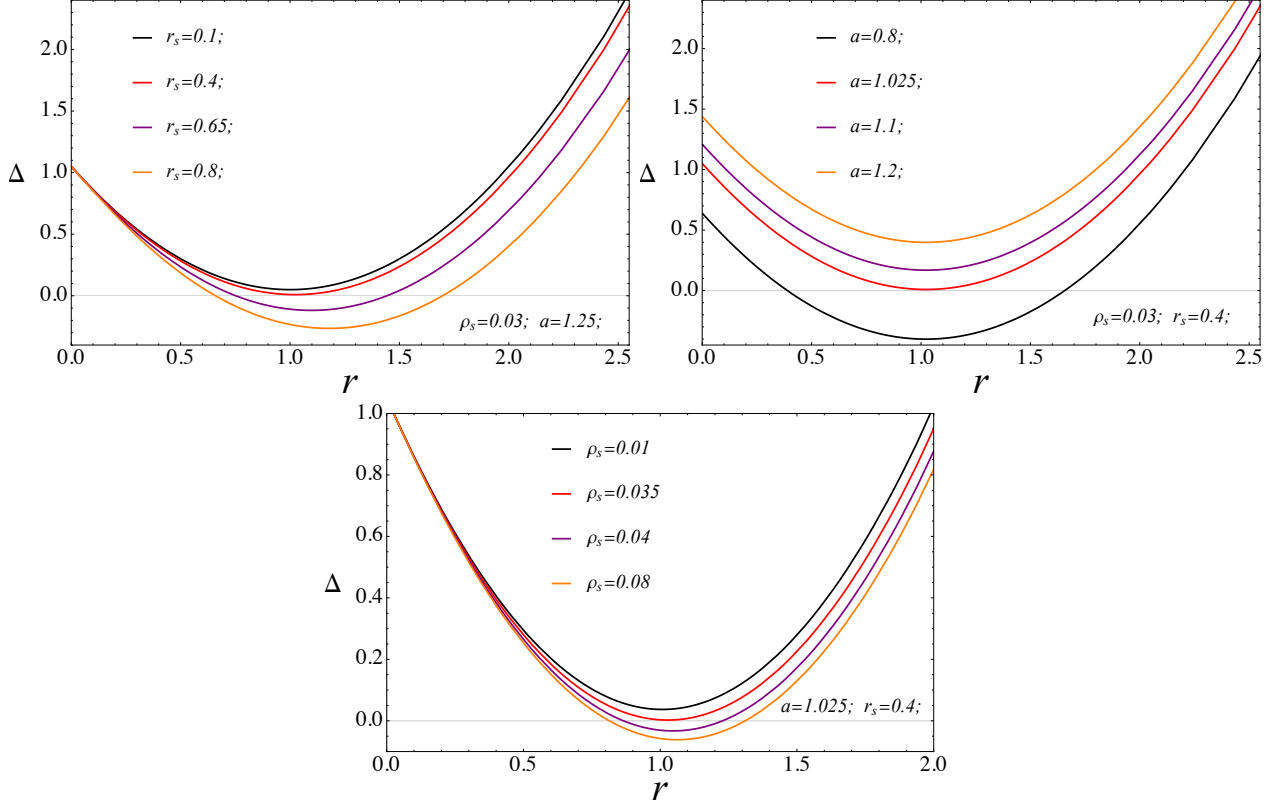


Figure 1: Radial dependence Δ function for different values of the BH parameters a , r_s , ρ_s

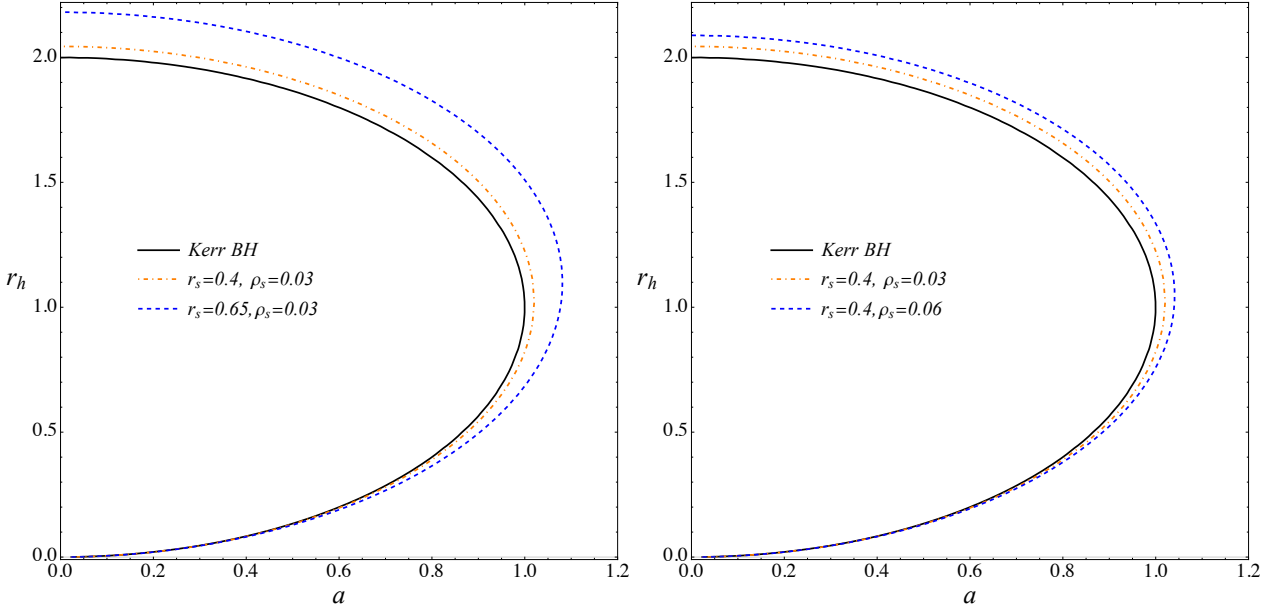


Figure 2: Variation of horizon radius with increase of BH spin parameter a for the selected values of parameters ρ_s , r_s . Hereafter, we shall for simplicity set $M = 1$.

of the BH, from the bottom panel of Fig.(1). Then, using condition $\Delta = 0$, we have plotted the dependence of the event horizon r_h on the spin parameter a for different values of characteristic density ρ_s and characteristic scale factor r_s of the DM halo in Fig. 2. One can easily notice that, from this graphic, increasing both BH parameters r_s and ρ_s causes an enlargement of the

values of the radii of the event horizon. This phenomenon can be interpreted as increasing the BH parameters r_s and ρ_s causes enlargement of the mass profile of the DM halo, which leads to enhanced gravitational mass.

2.1. Checking validity of the obtained rotating black hole solution

Now our aim is to check whether our obtained rotating black hole solution with dark matter halo satisfies the Einstein field

$$G_{tt} = -\frac{4F^2 + 2r[r^2 + a^2(2 - \cos^2 \theta)]F_{,r} - 2F[r^2 + a^2(2 - \cos^2 \theta) + 2rF_{,r}] - a^2 \sin^2 \theta \Sigma F_{,rr}}{\Sigma^3}, \quad (10a)$$

$$G_{rr} = -\frac{2(F - rF_{,r})}{\Sigma \Delta}, \quad G_{\theta\theta} = \frac{2(F - rF_{,r}) + \Sigma F_{,rr}}{\Sigma}, \quad (10b)$$

$$G_{t\phi} = -\frac{a \sin^2 \theta [4F(a^2 + r^2 + rF_{,r}) - 4F^2 - (a^2 + r^2)(4rF_{,r} - \Sigma^3 F_{,rr})]}{\Sigma^3}, \quad (10c)$$

$$G_{\phi\phi} = -\frac{\sin^2 \theta}{\Sigma^3} \{4a^2 \sin^2 \theta F^2 - F[2(a^2 + r^2)(r^2 + a^2[2 - \cos^2 \theta]) + 4a^2 r \sin^2 \theta F_{,r}] + (a^2 + r^2)[2rF_{,r}(r^2 + a^2(2 - \cos^2 \theta)) - (a^2 + r^2)\Sigma F_{,rr}]\}, \quad (10d)$$

where we have introduced a new variable as $F(r) = \frac{r^2[1-f(r)]}{2}$. The Einstein field equations $G_{\mu\nu} = 8\pi T_{\mu\nu}$ could then be checked using an appropriate form of orthogonal bases ([29, 33]) such as:

$$e_t^\mu = -\frac{(r^2 + a^2, 0, 0, a)}{\sqrt{\Sigma \Delta}}, \quad e_r^\mu = -\frac{\sqrt{\Delta}(0, 1, 0, 0)}{\sqrt{\Sigma}}, \quad (11a)$$

$$e_\theta^\mu = -\frac{(0, 0, 1, 0)}{\sqrt{\Sigma}}, \quad e_\phi^\mu = \frac{(a \sin^2 \theta, 0, 0, 1)}{\sqrt{\Sigma} \sin \theta}. \quad (11b)$$

Also, according to ([29, 34]) the components of the energy-momentum tensor $T_\mu^\nu = \text{diag}[-\rho, p_r, p_\theta, p_\phi]$ can be expressed as:

$$-\rho = p_r = \frac{(rF_{,r} - F)}{4\pi\Sigma^2}, \quad p_\theta = p_\phi = -p_r + \frac{F_{,rr}}{8\pi\Sigma}. \quad (12a)$$

Then one can easily notice that the newly obtained rotating black hole solution with a DM halo (8) satisfies the Einstein field equations indicating that the obtained line element is physically valid as $-\rho = \frac{1}{8\pi} e_t^\mu e_t^\nu G_{\mu\nu}$, $p_r = \frac{1}{8\pi} e_r^\mu e_r^\nu G_{\mu\nu} = \frac{1}{8\pi} g^{rr} G_{rr}$, $p_\theta = \frac{1}{8\pi} e_\theta^\mu e_\theta^\nu G_{\mu\nu} = \frac{1}{8\pi} g^{\theta\theta} G_{\theta\theta}$, $p_\phi = \frac{1}{8\pi} e_\phi^\mu e_\phi^\nu G_{\mu\nu}$.

3. Shadow of rotating black hole in Dehnen-type DM halo

To find the apparent shadow of the rotating BH with a Dehnen-type DM halo, we start by studying null geodesics. The equation of motion for a photon can be expressed with the Hamilton-Jacobi equations:

$$\frac{\partial S}{\partial \lambda} = -\frac{1}{2} g^{\mu\nu} \frac{\partial S}{\partial x^\mu} \frac{\partial S}{\partial x^\nu}, \quad (13)$$

where λ is the affine parameter. Then, using the separability of the Hamilton-Jacobi action:

$$S = -Et + L\phi + S_r(r) + S_\theta(\theta), \quad (14)$$

equations or not. Using the line element of the black hole surrounded by Dehnen-type DM halo (8,9), the components of the Einstein tensor can be expressed as:

where E and L are the energy and angular momentum of the particles, we can find the equation of motion as:

$$\Sigma \frac{dt}{d\lambda} = a(L - aE \sin^2 \theta) + \frac{r^2 + a^2}{\Delta} [E(r^2 + a^2) - aL], \quad (15a)$$

$$\Sigma \frac{dr}{d\lambda} = \pm \sqrt{R}, \quad (15b)$$

$$\Sigma \frac{d\theta}{d\lambda} = \pm \sqrt{\Theta}, \quad (15c)$$

$$\Sigma \frac{d\phi}{d\lambda} = (L \csc^2 \theta - aE) + \frac{a}{\Delta} [E(r^2 + a^2) - aL], \quad (15d)$$

in which

$$R = [(r^2 + a^2)E - aL]^2 - \Delta [\mathcal{K} + (L - aE)^2], \quad (16a)$$

$$\Theta = \mathcal{K} + \cos^2 \theta \left(a^2 E^2 - \frac{L^2}{\sin^2 \theta} \right). \quad (16b)$$

Here, \mathcal{K} is the separation constant. The following effective potential can be written as

$$\left(\Sigma \frac{dr}{d\lambda} \right)^2 + V_{eff} = 0, \quad (17a)$$

$$\frac{1}{E^2} V_{eff} = \Delta [\eta + (\xi - a)^2] - [(r^2 + a^2) - a\xi]^2, \quad (17b)$$

where we have introduced new variables $\eta = \frac{\mathcal{K}}{E^2}$ and $\xi = \frac{L}{E}$. Then we can use condition for unstable circular orbits $V_{eff}(r_{ph}) = \frac{\partial V_{eff}}{\partial r} |_{r_{ph}} = 0$, where r_{ph} [35] is the radius of the photon sphere, to find η and ξ as:

$$\xi = \frac{\Delta' (r^2 + a^2) - 4r\Delta}{a\Delta'}, \quad (18a)$$

$$\eta = \frac{r^2 [16\Delta(a^2 - \Delta) + 8r\Delta\Delta' - r^2\Delta'^2]}{a^2\Delta'^2}. \quad (18b)$$

Here, the prime ' denotes the derivative with respect to the radial coordinate r .

We will introduce new celestial coordinate systems α and β to investigate the dark region in the sky, the so-called black hole shadow:

$$\alpha = \lim_{r \rightarrow \infty} \left(-r^2 \sin \theta \frac{d\phi}{dr} \Big|_{\theta=\theta_0} \right) = -\xi \csc \theta_0, \quad (19a)$$

$$\beta = \lim_{r \rightarrow \infty} \left(r^2 \frac{d\theta}{dr} \Big|_{\theta=\theta_0} \right) = \pm \sqrt{a^2 \cos^2 \theta + \eta - \xi^2 \cot^2 \theta}, \quad (19b)$$

where θ_0 is the angle of inclination of the observer. For the BH shadow in the equatorial plane ($\theta_0 = \frac{\pi}{2}$) Eqs. (19) can be rewritten in the form:

$$\alpha = -\xi, \quad (20a)_{200}$$

$$\beta = \pm \sqrt{\eta}. \quad (20b)$$

Now, to obtain the silhouette of the BH shadow, one may plot the line described by ξ vs. η in celestial coordinates [36]. Then, in Fig. 3, we have shown the shadow of the rotating BH surrounded by a Dehnen-type dark matter halo. Again, from these graphs shown in 3, one can easily conclude that increasing the values of the BH parameters r_s and ρ_s leads to an increase in the shadow of the BH. In addition, the well-known effect of the spin a of the BH on the shadow, distortion of the shadow of the BH, is seen from the bottom panels of the graphics plotted in 3.

The expression for the shadow radius can be expressed as:

$$R_{sh}^2 = \alpha^2 + \beta^2, \quad (21)$$

Then, in Fig. 4 we have plotted the photon sphere and shadow radius for different spacetime parameters.

One can notice from Fig. 4 enlarging the values of both space-time parameters r_s and ρ_s causes increasing the radii of photon sphere r_p and the size of the shadow R_{sh} , which is coincide with the interpretation of the Fig. 3 we have done in above discussion.

4. Deflection angle of light by a rotating black hole in Dehnen-type DM halo.

In this section, we will study the deflection angle for a rotating black hole in Dehnen-type DM halo via OIA method ([37, 38]). To achieve this, we begin by applying the null condition $ds^2 = 0$ and derive the orbital equation in the equatorial plane, where $\theta = \frac{\pi}{2}$. We also utilize a bounded, two-dimensional orientable surface, as depicted in Fig. 5. Following, the geodesic constants, energy $E = -k_{(t)}^\mu p_\mu$ and angular momentum $L = k_{(\phi)}^\mu p_\mu$ in which:

$$k_t^\mu = (1, 0, 0, 0) \text{ timelike Killing vector,}$$

$$k_\phi^\mu = (0, 0, 0, 1) \text{ spacelike Killing vector,}$$

for the line element (8) can be expressed as:

$$E = -g_{tt}\dot{t} - g_{t\phi}\dot{\phi}, \quad (23a)$$

$$L = g_{t\phi}\dot{t} + g_{\phi\phi}\dot{\phi}, \quad (23b)$$

here dot means derivative with respect to affine parameter.

Subsequently, impact parameter b can be defined as:

$$b = \frac{L}{E} = \frac{g_{t\phi} + g_{\phi\phi} \frac{d\phi}{dt}}{-g_{tt} - g_{t\phi} \frac{d\phi}{dt}}, \quad (24)$$

which paves a way to find $\frac{dr}{d\phi}$ using condition $ds^2 = 0$ for the line element (8) as:

$$\left(\frac{dr}{d\phi} \right)^2 = \frac{(g_{t\phi}^2 - g_{tt}g_{\phi\phi})(b^2g_{tt} + 2bg_{t\phi} + g_{\phi\phi})}{g_{rr}(g_{tt}b + g_{t\phi})^2}, \quad (25)$$

or after introducing new variable as $u = \frac{1}{r}$ Eq. (25) can be rewritten as:

$$\left(\frac{du}{d\phi} \right)^2 = \frac{u^4(g_{t\phi}^2 - g_{tt}g_{\phi\phi})(b^2g_{tt} + 2bg_{t\phi} + g_{\phi\phi})}{g_{rr}(g_{tt}b + g_{t\phi})^2}. \quad (26)$$

Again, using the null condition $ds^2 = 0$ for metric (8) we are able to find dt as:

$$dt = \sqrt{\gamma_{ij}dx^i dx^j} + \beta_i dx^i, \quad (27a)$$

$$dl^2 = \gamma_{ij}dx^i dx^j = \frac{g_{t\phi}^2 - g_{\phi\phi}g_{tt}}{g_{tt}^2} d\phi^2 - \frac{g_{rr}}{g_{tt}} dr^2, \quad (27b)$$

$$\beta_i dx^i = -\frac{g_{t\phi}}{g_{tt}} d\phi, \quad (27c)$$

in which $\gamma_{ij} \neq g_{ij}$ ($i, j = 1, 2, 3$) is the spatial metric and l is the arc-length.

Then, on the equatorial plane the photon's path is described by a unit tangent vector e^i , given by([38],[37]):

$$e^i = \frac{1}{\chi} \left(\frac{dr}{d\phi}, 0, 1 \right), \quad (28)$$

in which χ can be obtained using condition $\gamma^i e^i = 1$ as

$$\frac{1}{\chi} = \frac{g_{tt}(g_{tt}b + g_{t\phi})}{g_{t\phi}^2 - g_{tt}g_{\phi\phi}}. \quad (29)$$

In the case where the unit radial vector is directed outgoing, we find:

$$R^i = \left(\frac{1}{\sqrt{\gamma_{rr}}}, 0, 0 \right), \quad (30)$$

which enables to find angle computed from the outgoing radial direction as:

$$\sin \Psi = -\frac{g_{t\phi} + bg_{tt}}{\sqrt{g_{t\phi}^2 - g_{tt}g_{\phi\phi}}}, \quad (31)$$

where we have used expression $\cos \Psi = \gamma_{ij} e^i R^j$. Eq.(31) can be expressed for metric (9) in the form:

$$\sin \Psi = \frac{b}{r} \times \frac{1 - \frac{2\tilde{M}}{r} + \frac{2a\tilde{M}}{br}}{\sqrt{1 - \frac{2\tilde{M}}{r} + \frac{a^2}{r^2}}}, \quad (32)$$

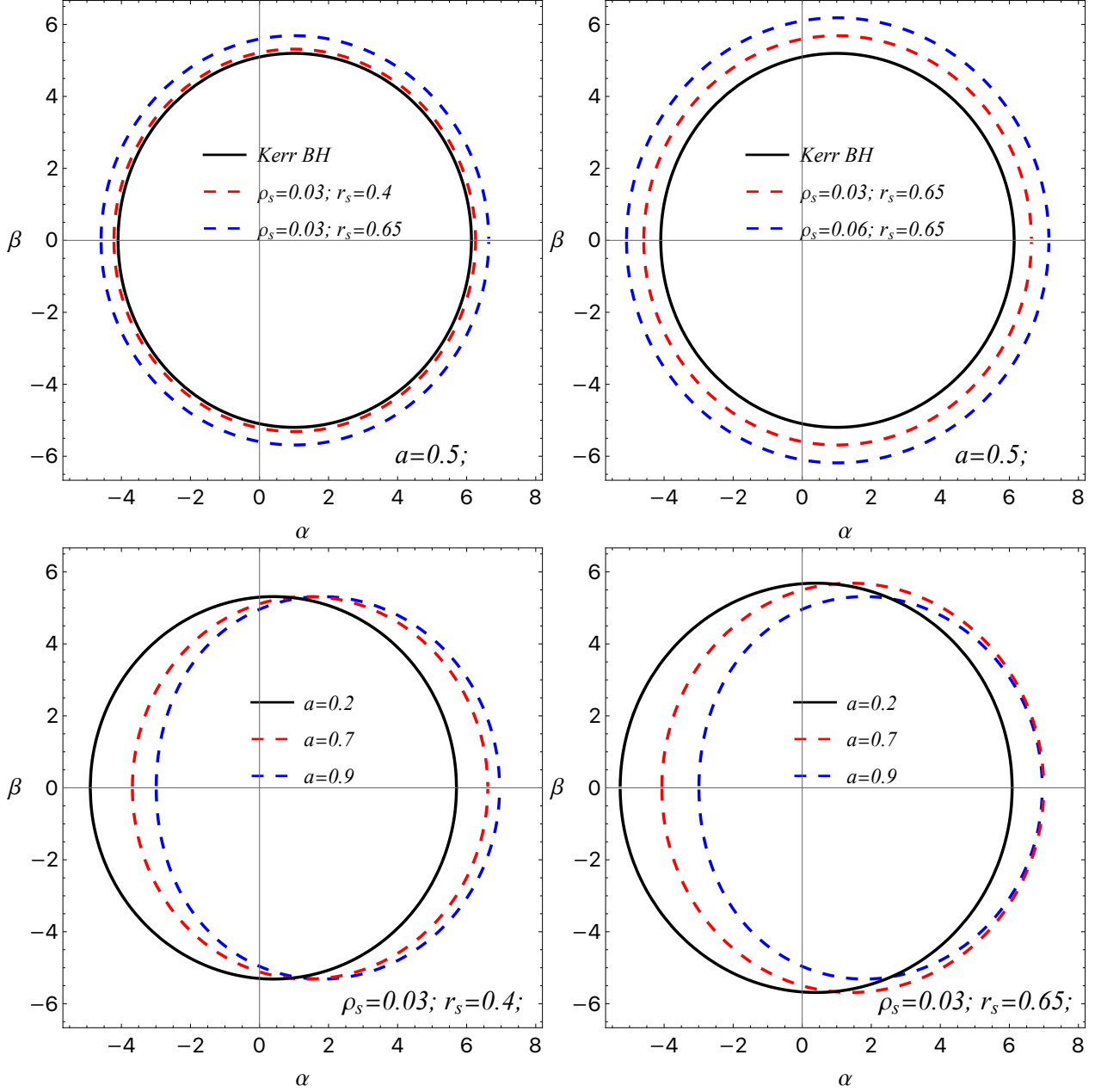


Figure 3: BH shadow for various of the BH parameters r_s, ρ_s, a .

here $\tilde{M} = \left[M + M_D \log \left(1 + \frac{r_s}{r} \right)^{1 + \frac{r_s}{r}} \right]$, eq.(32) converts to the exactly Kerr form ([37]) when $\rho_s \rightarrow 0$. Subsequently, eq.(32) can be approximated as:

$$\sin \Psi = \frac{b}{r} \left(1 - \frac{\tilde{M}}{r} + \frac{2a\tilde{M}}{br} \right) + \mathcal{O} \left(\frac{\tilde{M}^2}{r^2}, \frac{a^2}{r^2} \right). \quad (33)$$

Then we are able to obtain relation between the angles at the receiver Ψ_R and the source Ψ_S in the form:

$$\begin{aligned} \Psi_R - \Psi_S &= \arcsin(bu_R) + \arcsin(bu_S) - \pi - \\ &- \frac{\tilde{M}bu_R^2}{\sqrt{1-b^2u_R^2}} - \frac{\tilde{M}bu_S^2}{\sqrt{1-b^2u_S^2}} + \end{aligned} \quad (34)$$

$$+ \frac{2\tilde{M}u_R^2}{\sqrt{1-b^2u_R^2}} + \frac{2\tilde{M}u_S^2}{\sqrt{1-b^2u_S^2}}.$$

The deflection angle can now be formulated in terms of the newly defined angles at the receiver Ψ_R , the source Ψ_S , and the coordinate angle ϕ_{RS} as:

$$\hat{\alpha} = \Psi_R - \Psi_S + \phi_{RS}, \quad (35)$$

where ϕ_{RS} can be calculated employing Eq.(25) as:

$$\begin{aligned} \phi_{RS} &= \pi - \arcsin(bu_R) - \arcsin(bu_S) + \\ &+ \frac{2\tilde{M}^*}{b} \left[\frac{2-b^2u_R^2}{2\sqrt{1-b^2u_R^2}} + \frac{2-b^2u_S^2}{2\sqrt{1-b^2u_S^2}} \right] \end{aligned} \quad (36)$$

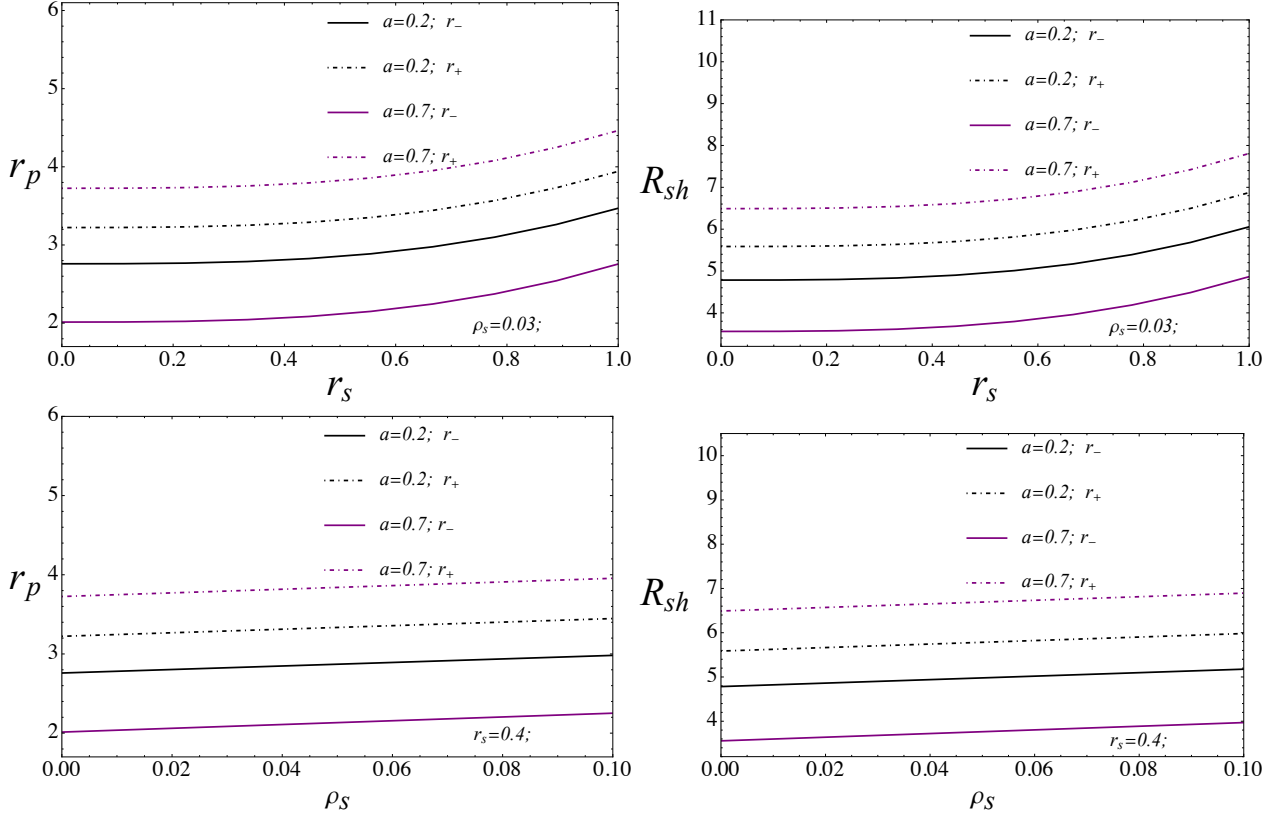


Figure 4: Dependence of the shadow size R_{sh} and photon sphere r_p with respect to different spacetime parameters, here r_{\pm} refers to the prograde and retrograde radii of stable circular orbits.

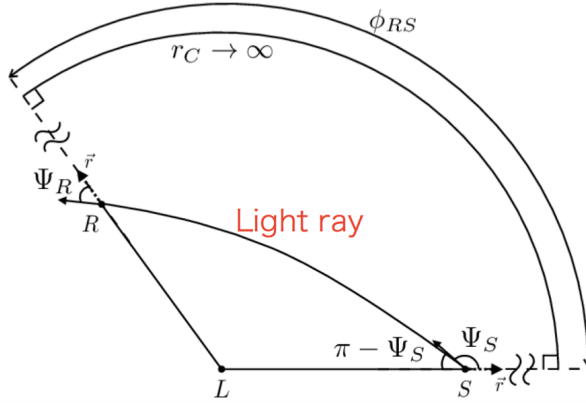


Figure 5: The geometry of a quadrilateral embedded in curved space is presented.[38]

$$- \frac{2a\tilde{M}^*}{b^2} \left[\frac{1}{\sqrt{1-b^2u_S^2}} + \frac{1}{\sqrt{1-b^2u_S^2}} \right],$$

here we used weak field and slow rotation approximations (see, ([37]), [39] for details).

Finally, taking far limit $r_S \rightarrow 0$, $r_R \rightarrow 0$ and substituting Eqs.(34) and (36) into Eq.(35) we will have expression for deflection angle:

$$\hat{\alpha} = \frac{4\tilde{M}^*}{b} \pm \frac{4a\tilde{M}^*}{b^2}, \quad (37)$$

where +, - signs here correspond to the retrograde and prograde photon orbits and $\tilde{M}^* \approx M + 4\pi\rho_s r_s^3$. Then we have shown how deflection angle $\hat{\alpha}$ depend on the impact parameter b in Fig.(6). One can see from graphics in Fig.(6) that presence of the DM halo increases the value of the deflection angle $\hat{\alpha}$.

5. Constraints from EHT observational data

Now we will obtain constraints from the observational data of the EHT on the image characteristics of SMBHs. To do it, we ought to find a closed area of the shadow silhouette as [40]

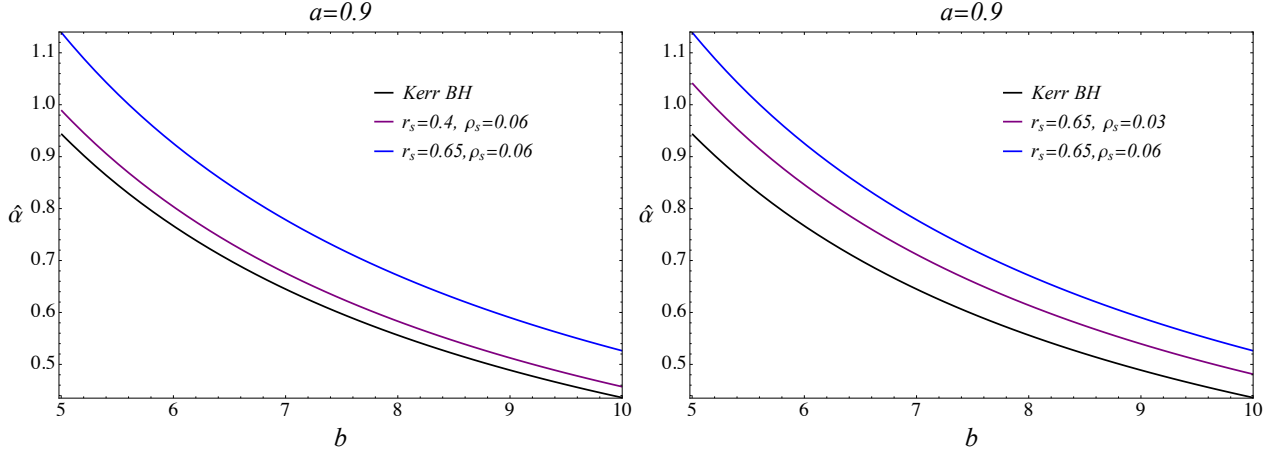


Figure 6: Dependence of the deflection angle $\hat{\alpha}$ on the impact parameter b for various cases.

([41]):

$$A = 2 \int_{r_-}^{r_+} \left[\beta(r) \frac{d\alpha(r)}{dr} \right] dr, \quad (38)$$

which enables us to find the radius of the areal shadow as $R_a = \sqrt{\frac{A}{\pi}}$.

Now we can determine the constraints for spacetime parameters of the supermassive black holes Sgr A* and M87*, assuming them as rotating black holes with a dark matter halo and using the angular diameter of their shadow image measured by EHT observation at a distance d from the black hole, which can be expressed as:

$$\Theta_d = 2 \frac{R_a}{d}. \quad (39)$$

The observational angular diameters of the shadow images of the SMBHs M87* and Sgr A* are $\Theta_d = 42 \pm 3 \mu\text{as}$ and $\Theta_d = 48.7 \pm 7 \mu\text{as}$, respectively ([42],[22]). We would like to point out that, for simplicity, we do not take into account the possible uncertainties in the mass and distance measurements of the black holes in the numerical estimations.

Then in the top panel of Fig. 7, we present the density plots of the characteristic scale r_s and characteristic density ρ_s of the black hole that are fitted with the measured values of the angular diameter of Sgr A*, where we assume the mass of SMBH SgrA* as $M \approx 4 \times 10^6 M_\odot$ and the distance from Earth to SMBH Sgr A* as $d \approx 8 \text{ kpc}$ ([22]), for the different fixed values of the BH spin a . To be more informative, we show the lower bound $\Theta_d = 41.7 \mu\text{as}$ (black curves on top panels of Fig. 7) and the mean value $\Theta_d = 48.7 \mu\text{as}$ (blue dashed lines on top panels of Fig. 7 of the angular diameter of the supermassive black hole Sgr A*. It is clear from Fig. 7 that the values of the BH parameters r_s and ρ_s should be relatively high to coincide with the EHT observational data for Sgr A*.

In addition, we performed the same analysis for the measured value of the angular diameter of SMBH M87* ([42]) in the bottom panel of Fig. 7. Again, we present the lower bound $\Theta_d = 39 \mu\text{as}$ (solid black lines in the bottom graphics of Fig. 7),

and mean value $\Theta_d = 42$ (blue dashed lines in the bottom panels of Fig. 7) of the angular diameter of the supermassive black hole M87*. Similarly, the characteristic scale r_s and the characteristic density ρ_s of the rotating BH in the dark matter halo have to be relatively high to coincide with the EHT observational data for M87*.

5.1. Parameter estimation for a rotating black hole in Dehnen-type DM halo through MCMC analysis

In this section we constrain DM parameter ρ_s , r_s and BH mass M , BH spin a employing MCMC analysis and using observed data for SgrA* from EHT collaboration ([42]), observed data for SgrA* from Gravity collaboration ([43]), observed data for M87* from EHT collaboration ([22]).

We start with posterior distribution:

$$P(\Theta|\mathcal{D}, \mathcal{M}) = \frac{\mathcal{L}(\Theta|\mathcal{D}, \mathcal{M}) \pi(\Theta|\mathcal{M})}{P(\mathcal{D}, \mathcal{M})}, \quad (40)$$

where the likelihood function $L(\Theta|\mathcal{D}, \mathcal{M})$ tells us how well the parameters Θ explain the data \mathcal{D} according to model \mathcal{M} :

$$\mathcal{L} = -\frac{1}{2} \sum_i \left(\frac{\theta_{obs.}^i - \theta_{th.}^i}{\sigma_i} \right)^2, \quad (41)$$

in which $\theta_{obs.}$ is the observed value of the angular shadow size of the BHs, $\theta_{th.}$ is the theoretical value (39) of the angular shadow size of the BHs.

Then we set the priors to be Gaussian priors, with boundary condition:

$$\pi(\Theta_i) \sim \exp \left[-\left(\frac{\Theta_i - \Theta_{0,i}}{\sigma_i} \right)^2 \right], \quad (42)$$

in which σ_i is the standard deviation. Subsequently, numerical values for the priors of the parameters of rotating BH in DM halo used in our analysis is given in Table (1).

Following, we constrain DM halo parameters ρ_s , r_s and BH mass M , BH spin a employing MCMC analysis and show visually in Fig.(8). Also, to be more informative we give numerical values of best-fit values for the parameters in Table(2).

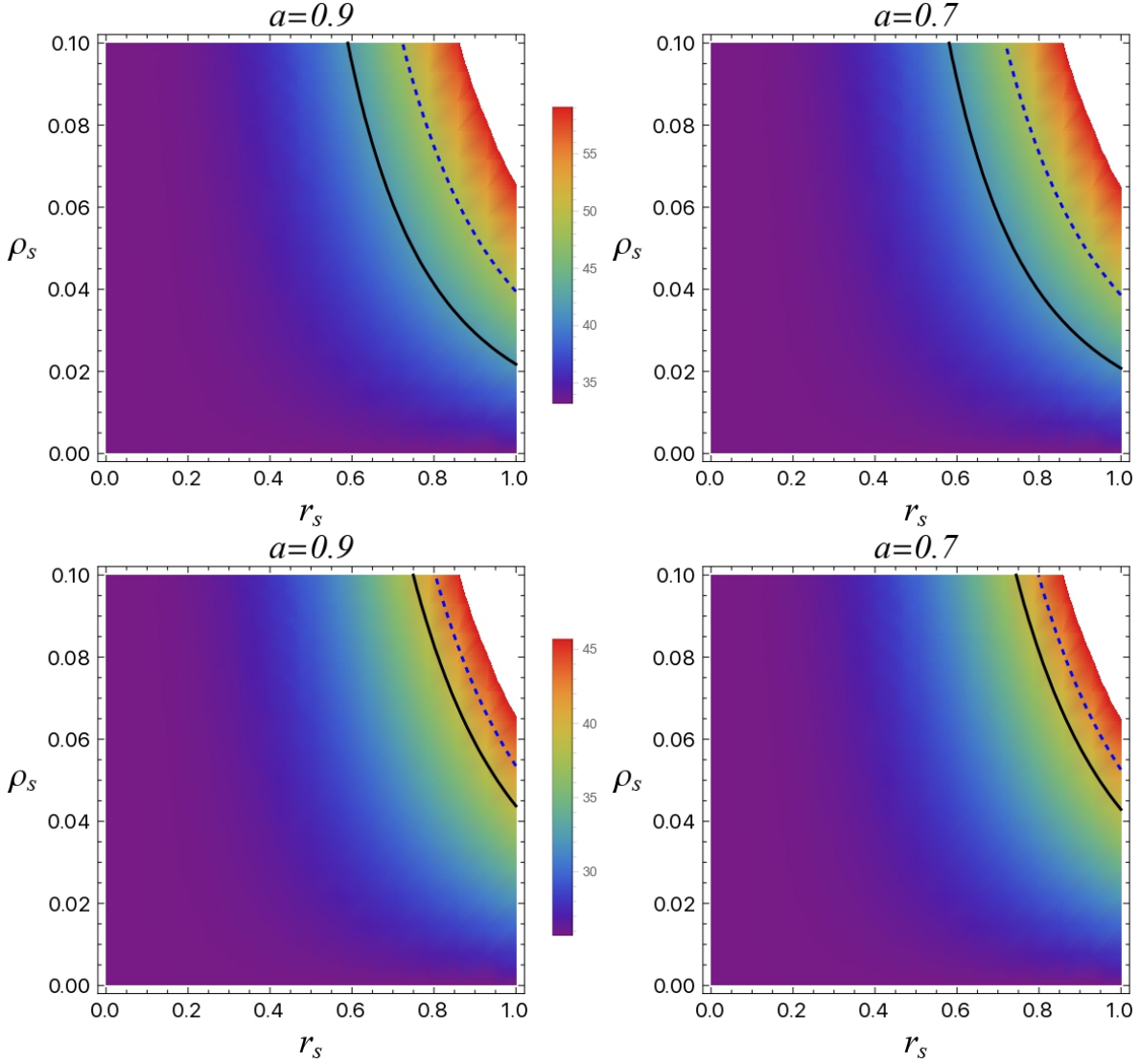


Figure 7: Angular diameter observable Θ_d for the black hole shadows as a function of parameters r_s and ρ_s . The black curves correspond to $\Theta_d = 41.7\mu\text{as}$ (for top panels) and $\Theta_d = 39\mu\text{as}$ (for bottom panels) within 1σ region of the measured angular diameter, $\Theta_d = 48.7 \pm 7\mu\text{as}$, of the *SgrA** black hole (top panels) and $\Theta_d = 42 \pm 3\mu\text{as}$ of the *M87** black hole reported by the EHT. The blue dashed curve corresponds to $48.7\mu\text{as}$ and $42\mu\text{as}$, respectively.

	<i>SgrA*</i> from EHT		<i>SgrA*</i> from Gravity		<i>M87*</i> from EHT	
	μ	σ	μ	σ	μ	σ
M [$\times 10^6 M_\odot$]	4.25	0.6	4.1	0.6	6300	250
r_s [$10^{17} M_\odot$]	0.8	0.15	0.8	0.2	1.6	0.21
ρ_s [$1/10^{19} M_\odot^2$]	0.255	0.005	0.0326	0.005	0.004	0.0007
a [M]	0.9	0.15	0.9	0.16	1	0.1

Table 1: Gaussian prior on rotating BHs in Dehnen-type DM halo from angular shadow size constraints.

Our derived best-fit parameters for the dark matter halo show well agreement with values reported in prior studies (see for example, [44]) as:

$$\rho_s \sim \frac{10^{-2}}{(10^{19} M_\odot)^2} \frac{c^6}{G^3} \sim 10^{-24} g/cm^3, \quad (43)$$

$$r_s \sim 10^{17} M_\odot \frac{G}{c^2} \sim 10^{22} cm \sim 10 \text{kpc}.$$

	<i>SgrA*</i> from EHT	<i>SgrA*</i> from Gravity	<i>M87*</i> from EHT
M ($\times 10^6 M_\odot$)	$4.057^{+0.563}_{-0.528}$	$4.087^{+0.605}_{-0.537}$	$6.431^{+0.438}_{-0.442} \times 10^3$
r_s [$10^{16} M_\odot$]	$0.784^{+0.145}_{-0.121}$	$0.802^{+0.178}_{-0.132}$	$1.6^{+0.210}_{-0.208}$
ρ_s [$1/10^{19} M_\odot^2$]	$0.025^{+0.005}_{-0.005}$	$0.033^{+0.005}_{-0.005}$	$0.004^{+0.001}_{-0.001}$
a [M]	$0.899^{+0.147}_{-0.146}$	$0.9^{+0.149}_{-0.150}$	$1^{+0.100}_{-0.099}$

Table 2: Best-fit rotating BHs in DM halo parameters derived from angular shadow size.

6. Thin accretion disk

Now we aim to get a simulation of a geometrically thin infinite accretion disk in a rotating BH surrounded by a DM halo spacetime (8). To achieve our intention, we have modified the open source Gyoto ray-tracing code ([45]) to adapt the code to our obtained spacetime (8).

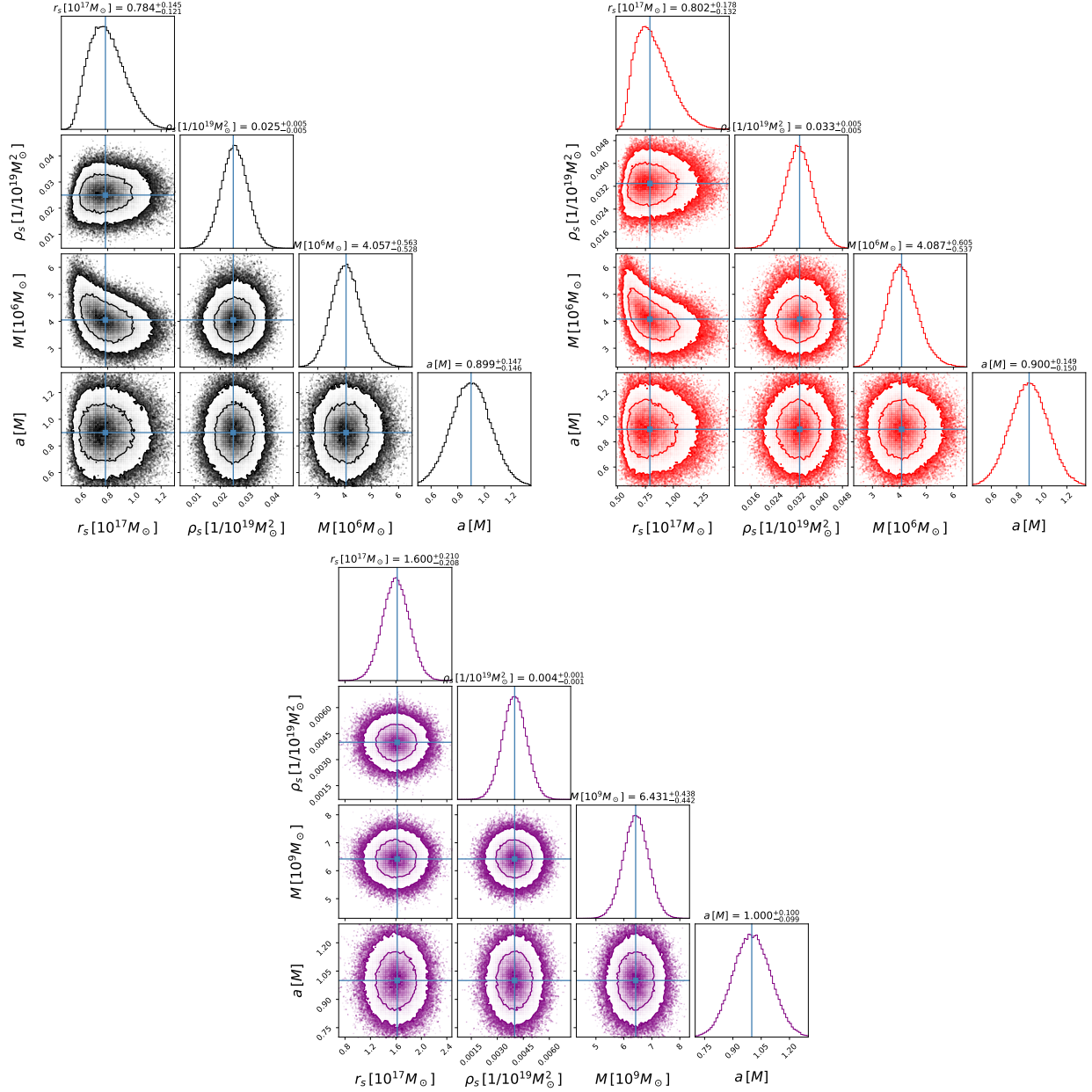


Figure 8: MCMC for Sgr A* from EHT (top left), Sgr A* from Gravity (top right), M 87* from EHT (bottom).

Finding innermost stable circular orbits (ISCO) is an important step to analyze the thin accretion disk of the rotating BH in DM halo ([46]). To do it we start with expressing the effective potential of the massive particle in the vicinity of a rotating BH surrounded by Dehnen-type DM halo ([47]):

$$V_{m,eff} = \frac{g_{t\phi}}{g_{\phi\phi}} l + \sqrt{\left(\frac{g_{t\phi}^2}{g_{\phi\phi}} - g_{tt}\right) (1 + g^{\phi\phi} l^2)}, \quad (44)$$

where $l = \frac{L}{m}$ is the specific angular momentum of the test particle. Then the ISCO position can be found using the condi-

tion:

$$V_{m,eff} = \frac{\partial V_{m,eff}}{\partial r} = \frac{\partial^2 V_{m,eff}}{\partial r^2} = 0. \quad (45)$$

Then, solving Eq.(45) numerically, we have plotted how the ISCO radius depends on the DM halo parameters ρ_s and r_s for different cases in Fig.9. It is obvious from Fig.9 that increasing both DM halo parameters ρ_s and r_s leads to the enlargement of the value of the ISCO radius r_{ISCO} since the DM halo causes the mass of the BH-DM system.

The flux of electromagnetic radiation can be expressed as ([48–52]):

$$\mathcal{F}(r) = -\frac{\dot{M}_0}{4\pi} \frac{\Omega_r}{\sqrt{-g} (E - \Omega L)^2} \int_{r_{ISCO}}^r (E - \Omega L) L_r dr, \quad (46)$$

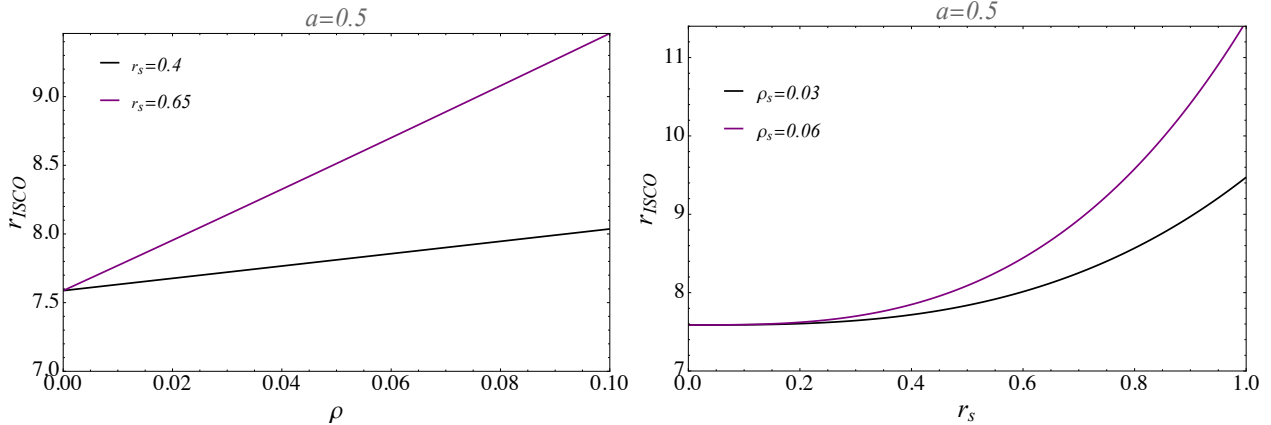


Figure 9: The dependence of the ISCO radius on the parameters of the DM halo ρ_s and r_s for different cases.

here \dot{M}_0 is the accretion rate, g is the determinant of the three-dimensional subspace.

Then, in Fig.10 we have plotted the image thin accretion disk in a rotating BH surrounded by a Dehnen-type DM halo for different values of the DM parameters ρ_s and r_s for the angle of inclination $\theta_0 = \frac{\pi}{10}$. One can notice by comparing images of the thin accretion disks of the obtained rotating BHs with thin accretion disks of Kerr and Schwarzschild BHs in Fig.10, that increasing both DM halo parameters ρ_s and r_s causes decreasing the value of the radiation flux as these parameters ρ_s , r_s lead to growing the mass of the BH-DM system, so extending gravity around rotating BH in the DM halo.

7. Conclusion

The Event Horizon Telescope (EHT) observations of the shadows of supermassive black holes, like Sgr A* at the Milky Way's center and M87* in the nearby Messier 87 galaxy, provide an exceptional and natural laboratory for studying the gravitational properties of spacetime geometry around black holes, allowing tests in both strong and weak gravitational field regimes. In this work, we have generated a rotating BH space-time in a dark matter halo by applying the NJA method to the static spacetime metric and the components of the obtained metric tensor are provided in (8). Then the dependence of the horizon radius on the BH spin a is shown in Fig. 2 for different values of the characteristic density ρ_s and the characteristic scale factor r_s . It is shown that increasing spacetime parameters r_s and ρ_s causes an enlargement of the horizon radius of the rotating BH in a dark matter halo.

We have also studied the shadow cast by the spinning axially symmetric black hole surrounded by a Dehnen-type dark matter halo. Using the Hamilton-Jacobi equation, we found photon motion in the vicinity of the rotating BH in a dark matter halo, which enabled us to find the photon sphere r_{ph} and the shadow radius. The results obtained showed that the presence of the dark-matter halo causes an enlarged shadow as presented in Fig. 3.

Additionally, we have analyzed the photon sphere and shadow

radius of the rotating BH in a dark matter halo by giving numerical values of the photon sphere and shadow radius in Fig. 4.

To strengthen our pure theoretical analysis, we got constraints for BH parameters ρ_s and r_s from EHT observational data for spacetime parameters of supermassive black holes SgrA* and M87* in Sec. 5. Our provided analysis for the angular diameter Θ_d demonstrates that the characteristic density ρ_s and the characteristic scale factor r_s of the rotating BH in the Dehnen-type dark matter halo should be relatively high to fit the EHT observed data of the SMBHs images (look to Fig.7).

One may conclude from the performed study that the influence of a Dehnen-type dark matter halo in the environment of supermassive black holes Sgr A* and M87* can not be excluded. To be more precise, we perform MCMC analysis to constrain DM parameters ρ_s , r_s and BH mass M , BH spin a and it is presented that obtained best-fit values for the DM parameters ρ_s and r_s are well agreement with values showed in prior studies.

Finally, in Sec. 6 we have analyzed thin accretion disk in a new BH surrounded by a DM halo and give an image of the thin accretion disk in Fig.10. It was found that increasing DM parameters ρ_s and r_s causes a growing mass of the BH-DM system so leading to a decrease in the value of the electromagnetic radiation.

8. Acknowledgement

S.S. is supported by the National Natural Science Foundation of China under Grant No. W2433018.

References

- [1] B. P. Abbott *et al.* (LIGO Scientific, Virgo), *Phys. Rev. Lett.* **116**, 061102 (2016), arXiv:1602.03837 [gr-qc] .
- [2] B. P. Abbott and J. D. E. Abbott, *Phys. Rev. Lett.* **116**, 241102 (2016), arXiv:1602.03840 [gr-qc] .
- [3] F. Iocco, M. Pato, and G. Bertone, *Nat. Phys.* **11**, 245 (2015), arXiv:1502.03821 [astro-ph.GA] .

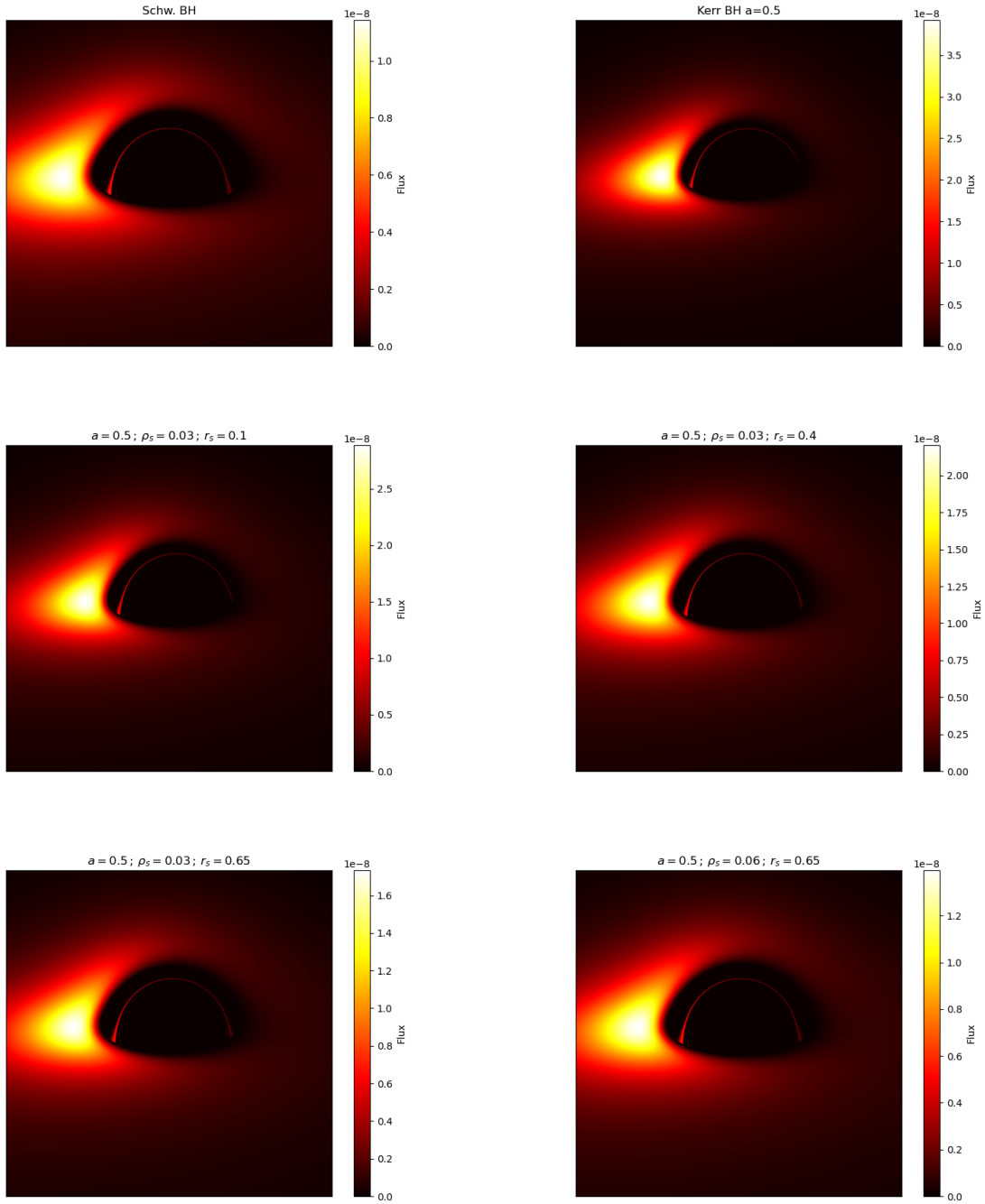


Figure 10: The images of the thin accretion disk in Schwarzschild BH, Kerr BH and rotating BH immersed in Dehnen-type DM halo spacetime with the observational angle $\theta_0 = \frac{\pi}{10}$.

[4] G. Bertone and T. M. P. Tait, *Nature* **562**, 51 (2018), [arXiv:1810.01668 \[astro-ph.CO\]](https://arxiv.org/abs/1810.01668) .

[5] A. W. Graham, D. Merritt, B. Moore, J. Diemand, and B. Terzic, *Astron. J.* **132**, 2701 (2006), [arXiv:astro-ph/0608613](https://arxiv.org/abs/astro-ph/0608613) .

[6] J. F. Navarro, C. S. Frenk, and S. D. M. White, *Astrophys. J.* **462**, 563 (1996), [arXiv:astro-ph/9508025 \[astro-ph\]](https://arxiv.org/abs/astro-ph/9508025) .

[7] A. Burkert, *Astrophys. J. Lett.* **447**, L25 (1995), [arXiv:astro-ph/9504041 \[astro-ph\]](https://arxiv.org/abs/astro-ph/9504041) .

[8] W. Dehnen, *Mon. Not. R. Astron. Soc.* **265**, 250 (1993).

[9] B. Shukirgaliyev, A. Otebay, M. Sobolenko, M. Ishchenko, O. Borodina, T. Panamarev, S. Myrzakul, M. Kalambay, A. Naurzbayeva, E. Abdikamalov, E. Polyachenko, S. Banerjee, P. Berczik, R. Spurzem,

- and A. Just, *Astron. Astrophys.* **654**, A53 (2021), [arXiv:2105.09510 \[astro-ph.GA\]](#) .
- [10] A. Al-Badawi, S. Shaymatov, and Y. Sekhmani, *JCAP* **02**, 014 (2025), [arXiv:2411.01145 \[gr-qc\]](#) .
- [11] K.-i. Maeda, V. Cardoso, and A. Wang, *Phys. Rev. D* **111**, 044060 (2025), [arXiv:2410.04175 \[gr-qc\]](#) .
- [12] Z. Shen, A. Wang, and S. Yin, *Phys. Lett. B* **862**, 139300 (2025), [arXiv:2408.05417 \[gr-qc\]](#) .
- [13] Z. Shen, A. Wang, Y. Gong, and S. Yin, *Phys. Lett. B* **855**, 138797 (2024), [arXiv:2311.12259 \[gr-qc\]](#) .
- [14] T. Xamidov, S. Shaymatov, Q. Wu, and T. Zhu, *Eur. Phys. J. C* **85**, 1193 (2025), [arXiv:2507.13147 \[gr-qc\]](#) .
- [15] M. Alloqulov, T. Xamidov, S. Shaymatov, and B. Ahmedov, *arXiv e-prints* , [arXiv:2504.05236 \(2025\)](#), [arXiv:2504.05236 \[gr-qc\]](#) .
- [16] M. M. Gohain, P. Phukon, and K. Bhuyan, *Phys. Dark Universe* **46**, 101683 (2024), [arXiv:2407.02872 \[gr-qc\]](#) .
- [17] T. Xamidov, U. Uktamov, S. Shaymatov, and B. Ahmedov, *Phys. Dark Universe* **47**, 101805 (2025).
- [18] S. Vagnozzi and L. Visinelli, *Phys. Rev. D* **100**, 024020 (2019).
- [19] C. Bambi, K. Freese, S. Vagnozzi, and L. Visinelli, *Phys. Rev. D* **100**, 044057 (2019), [arXiv:1904.12983 \[gr-qc\]](#) .
- [20] S. Vagnozzi, R. Roy, Y.-D. Tsai, L. Visinelli, M. Afrin, A. Allahyari, P. Bambhaniya, D. Dey, S. G. Ghosh, P. S. Joshi, K. Jusufi, M. Khodadi, R. K. Walia, A. Övgün, and C. Bambi, *Classical and Quantum Gravity* **40**, 165007 (2023), [arXiv:2205.07787 \[gr-qc\]](#) .
- [21] K. Akiyama and et al. (Event Horizon Telescope Collaboration), *Astrophys. J.* **875**, L1 (2019), [arXiv:1906.11238 \[astro-ph.GA\]](#) .
- [22] K. Akiyama and et al. (Event Horizon Telescope Collaboration), *Astrophys. J. Lett.* **930**, L12 (2022).
- [23] V. Cardoso and P. Pani, *Living Rev. Relativ.* **22**, 4 (2019), [arXiv:1904.05363 \[gr-qc\]](#) .
- [24] M. Zahid, S. U. Khan, J. Ren, and J. Rayimbaev, *Int. J. Mod. Phys. D* **31**, 2250058 (2022).
- [25] M. Zubair, M. A. Raza, and G. Abbas, *Eur. Phys. J. C* **82**, 948 (2022), [arXiv:2210.13750 \[gr-qc\]](#) .
- [26] M. A. Raza, M. Zubair, and E. Maqsood, *J. Cosmol. Astropart. Phys.* **2024**, 047 (2024), [arXiv:2401.04779 \[gr-qc\]](#) .
- [27] U. Uktamov, S. Shaymatov, B. Ahmedov, and C. Yuan, *Eur. Phys. J. C* **85**, 1432 (2025).
- [28] B. Toshmatov, C. Bambi, B. Ahmedov, A. Abdujabbarov, and Z. Stuchlík, *Eur. Phys. J. C* **77**, 542 (2017), [arXiv:1702.06855 \[gr-qc\]](#) .
- [29] M. Azreg-Aïnou, *Phy.Rev.D* **90**, 064041 (2014), [arXiv:1405.2569 \[gr-qc\]](#) .
- [30] M. Azreg-Aïnou, *Eur. Phys. J. C* **74**, 2865 (2014), [arXiv:1401.4292 \[gr-qc\]](#) .
- [31] M. Azreg-Aïnou, *Physics Letters B* **730**, 95 (2014), [arXiv:1401.0787 \[gr-qc\]](#) .
- [32] E. T. Newman and A. I. Janis, *Journal of Mathematical Physics* **6**, 915 (1965).
- [33] K. Jusufi, M. Jamil, P. Salucci, T. Zhu, and S. Haroon, *Phys. Rev. D* **100**, 044012 (2019), [arXiv:1905.11803 \[physics.gen-ph\]](#) .
- [34] A. Burinskii, E. Elizalde, S. R. Hildebrandt, and G. Magli, *Phys. Rev. D.* **65**, 064039 (2002), [arXiv:gr-qc/0109085 \[gr-qc\]](#) .
- [35] M. Khodadi, S. Vagnozzi, and J. T. Firouzjaee, *Scientific Reports* **14**, 26932 (2024), [arXiv:2408.03241 \[gr-qc\]](#) .
- [36] N. Tsukamoto, Z. Li, and C. Bambi, *JCAP* **06**, 043 (2014), [arXiv:1403.0371 \[gr-qc\]](#) .
- [37] T. Ono, A. Ishihara, and H. Asada, *Phys. Rev. D* **96**, 104037 (2017), [arXiv:1704.05615 \[gr-qc\]](#) .
- [38] A. Övgün, İ. Sakallı, and J. Saavedra, *Annals Phys.* **411**, 167978 (2019), [arXiv:1806.06453 \[gr-qc\]](#) .
- [39] A. Ishihara, Y. Suzuki, T. Ono, T. Kitamura, and H. Asada, *Phys. Rev. D* **94**, 084015 (2016), [arXiv:1604.08308 \[gr-qc\]](#) .
- [40] M. Zahid, J. Rayimbaev, F. Sarikulov, S. U. Khan, and J. Ren, *Eur. Phys. J. C* **83**, 855 (2023).
- [41] A. A. Abdujabbarov, L. Rezzolla, and B. J. Ahmedov, *Mon. Not. R. Astron. Soc.* **454**, 2423 (2015), [arXiv:1503.09054 \[gr-qc\]](#) .
- [42] Event Horizon Telescope Collaboration, K. Akiyama, and et al., *Astrophys. J. Lett* **875**, L1 (2019), [arXiv:1906.11238 \[astro-ph.GA\]](#) .
- [43] R. Abuter *et al.* (GRAVITY), *Astron. Astrophys.* **657**, L12 (2022), [arXiv:2112.07478 \[astro-ph.GA\]](#) .
- [44] M. Cautun, A. Benitez-Llambay, A. J. Deason, C. S. Frenk, A. Fattahi, F. A. Gómez, R. J. J. Grand, K. A. Oman, J. F. Navarro, and C. M. Simpson, *Mon. Not. Roy. Astron. Soc.* **494**, 4291 (2020), [arXiv:1911.04557 \[astro-ph.GA\]](#) .
- [45] F. H. Vincent, T. Paumard, E. Gourgoulhon, and G. Perrin, *Classical and Quantum Gravity* **28**, 225011 (2011), [arXiv:1109.4769 \[gr-qc\]](#) .

- [46] J.-A. Marck, [Classical and Quantum Gravity](#) **13**, 393 (1996), [arXiv:gr-qc/9505010 \[gr-qc\]](#) .
- [47] S. U. Khan, U. Uktamov, J. Rayimbaev, A. Abdujabbarov, I. Ibragimov, and Z.-M. Chen, [Eur. Phys. J. C](#) **84**, 203 (2024).
- [48] U. Uktamov, M. Alloqulov, S. Shaymatov, T. Zhu, and B. Ahmedov, [Phys. Dark Univ.](#) **47**, 101743 (2025), [arXiv:2412.01809 \[gr-qc\]](#) .
- [49] M. Alloqulov, S. Shaymatov, B. Ahmedov, and A. Jawad, [Chinese Physics C](#) **48** (2024), [10.1088/1674-1137/ad137f](#).
- [50] M. Alloqulov and S. Shaymatov, [European Physical Journal Plus](#) **139** (2024), [10.1140/epjp/s13360-024-05524-1](#).
- [51] M. Alloqulov, M. Jamil, S. Shaymatov, Q. Wu, and M. Azreg-Aïnou, [Journal of High Energy Astrophysics](#) **48** (2025), [10.1016/j.jheap.2025.100424](#).
- [52] M. Alloqulov, A. Abdujabbarov, B. Ahmedov, C. Yuan, and C. Zhou, [European Physical Journal C](#) **85** (2025), [10.1140/epjc/s10052-025-14514-1](#).